CrossMark

Hydrogen pickup measurements in zirconium alloys: Relation to oxidation kinetics

Adrien Couet [a,*], Arthur T. Motta [a], Robert J. Comstock [b]

[a] Department of Mechanical and Nuclear Engineering, Penn State University, University Park, PA 16802, USA
[b] Westinghouse Electric Company, Pittsburgh, PA 15235, USA

ABSTRACT

The optimization of zirconium-based alloys used for nuclear fuel cladding aims to reduce hydrogen pickup during operation, and the associated cladding degradation. The present study focuses on precisely and accurately measuring hydrogen pickup fraction for a set of alloys to specifically investigate the effects of alloying elements, microstructure and corrosion kinetics on hydrogen uptake. To measure hydrogen concentrations in zirconium alloys two techniques have been used: a destructive technique, Vacuum Hot Extraction, and a non-destructive one, Cold Neutron Prompt Gamma Activation Analysis. The results of both techniques show that hydrogen pickup fraction varies significantly with exposure time and between alloys. A possible interpretation of the results is that hydrogen pickup results from the need to balance charge. That is, the pickup of hydrogen shows an inverse relationship to oxidation kinetics, indicating that, if transport of charged species is rate limiting, oxide transport properties such as oxide electronic conductivity play a key role in the hydrogen pickup mechanism. Alloying elements (either in solid solution or in precipitates) would therefore impact the hydrogen pickup fraction by affecting charge transport.

© 2014 Elsevier B.V. All rights reserved.

1. Introduction

Uniform corrosion of zirconium alloy fuel cladding and the associated hydrogen pickup is a potential life-limiting degradation mechanism for nuclear fuel cladding in existing and advanced light water reactors, since hydrogen ingress can cause cladding embrittlement [1]. Thus, it is of great interest to fuel vendors and utilities to limit cladding embrittlement both by decreasing the overall corrosion and by decreasing the amount of hydrogen ingress for a given corrosion rate [2,3]. It has been pointed out that several factors can affect the uniform corrosion of zirconium alloys [4]. Optimization of alloying elements is one of the key factors to obtain a zirconium-based alloy that is resistant to corrosion and that has low hydrogen pickup. Although extensive empirical knowledge is available, a mechanistic understanding of the role of alloying elements in the corrosion and hydrogen pickup mechanisms is still lacking [5–8].

The corrosion reaction is given by:

$$Zr + 2H_2O \rightarrow ZrO_2 + 2H_2 \tag{1}$$

A fraction of the hydrogen generated by the corrosion reaction (second term on the RHS of the above equation) diffuses through the protective oxide and enters the metal [2]. To compare the hydrogen pickup of different alloys, it is necessary to quantify the amount of hydrogen picked up relative to the amount of corrosion. To accomplish this, the hydrogen picked up by the metal during reactor or autoclave exposure is normalized to the total hydrogen generated in the corrosion reaction. The hydrogen pickup fraction f_H is defined as the ratio of the hydrogen absorbed by the metal over the total hydrogen generated in the corrosion reaction:

$$f_H = \frac{H_{absorbed}}{H_{generated}} \tag{2}$$

There is evidence that f_H depends strongly on alloying element additions [5,7], alloy microstructure and microchemistry [9,10] and corrosion conditions [11]. The small addition of alloying elements generally decreases hydrogen pickup with the notable exception of Ni which was eliminated from Zircaloy 4 for its role in increasing hydrogen pickup [7,12,13]. In addition, there is evidence that f_H changes during the corrosion process, such that different hydrogen pickup fractions are observed at different stages of oxide film growth [14].

* Corresponding author. Tel.: +1 814 865 9709.
E-mail address: adrien.couet@gmail.com (A. Couet).

This study is aimed at investigating the mechanistic link between hydrogen pickup, oxidation kinetics, alloy chemistry, and microstructure in zirconium alloys. Systematic measurements of hydrogen pickup and oxide growth were performed as a function of exposure time for an especially chosen set of zirconium alloys with specific compositions and microstructures. The precise hydrogen content at different exposure times was determined using two methods: a new technique called Cold Neutron Prompt Gamma Activation Analysis (CNPGAA) performed at the National Institute of Standards and Technology (NIST) and a conventional method, i.e. Vacuum Hot Extraction (VHE). CNPGAA has been shown to be reliable and precise by comparing its results with common destructive techniques such as VHE or Inert Gas Fusion [15].

Using these techniques, the total and *instantaneous*[1], hydrogen pickup fractions in zirconium alloys were systematically measured as a function of exposure time. The derived dependencies of the hydrogen pickup fraction on alloying element contents, alloy microstructure and exposure time are discussed.

2. Experimental procedures

2.1. Alloys

Alloys currently used in the industry such as Zircaloy-4 and ZIRLO[®2] were selected for this study along with Zr–2.5Nb, Zr–2.5Nb–0.5Cu, and three model alloys: pure Zr, Zr–0.5Cu and Zr–0.4Fe–0.2Cr to help understand the specific effect of alloying microstructure and composition on hydrogen pickup. All alloys were in the recrystallized state (RX) except for Zircaloy-4 tube which was in a cold-worked stress relieved state (CWSR). The full list of samples is detailed in Table 1. The starting hydrogen concentrations in the alloys prior to autoclave testing was 10–15 wt ppm.

The zirconium model alloys were processed from button ingots in a laboratory to sheet following the sequence of steps listed in Table 2. The buttons were rolled at different temperatures depending on the desired final microstructure. The sand blasted and pickled hot rolled strip was then vacuum annealed. This was followed by two iterations of cold rolling and vacuum annealing to produce final strip in a fully recrystallized condition with a thickness of about 0.8 mm. The majority of the alloys were processed at 580 °C. This was required in order to limit grain growth for commercially pure zirconium (sponge) and precipitate size in Zr–0.4Fe–0.2Cr (L) and Zr–0.5Cu alloys. A high process temperature of 720 °C was used to grow larger precipitates in the Zr–0.4Fe–0.2Cr (H) alloy.

In addition to the model alloys, several alloys were processed in both tubing and sheet form in production facilities. ZIRLO, Zircaloy-4, Zr–2.5Nb and Zr–2.5Nb–0.5Cu tube extrusions were processed to tubing following the procedure in [16]. The processing of ZIRLO and Zircaloy-4 tubing material was similar to that of sheet with multiple iterations of cold pilgering and annealing to final size.

The final microstructure of the alloys was studied by polarized light microscopy and scanning electron microscope (SEM) using secondary electron mode (Figs. 1–4) after polishing and etching of cross sectional samples using a 50 mL H_2O/45 mL HNO_3/5 mL HF solution. Energy Dispersive Spectroscopy (EDS) was performed to confirm precipitate type.

The etching reveals the precipitates and the grain structure. The micrographs show predominantly equiaxed grains and a homogeneous microstructure, as would be expected from a recrystallizing

Table 1
Description of the chemical composition, geometry and process temperature of the alloys used in this study.

Alloy system	Alloy composition (wt%)	Sample geometry	Process temperature °C
Pure Zr	Zr sponge	Sheet	580
Zr–Fe–Cr	Zr–0.4Fe–0.2Cr (L)	Sheet	(L): 580
	Zr–0.4Fe–0.2Cr (H)		(H): 720
Zr–Cu	Zr–0.5Cu	Sheet	580
Zr–Nb	Zr–2.5Nb	Tube	
Zr–Nb–Cu	Zr–2.5Nb–0.5Cu	Tube	580 [49]
ZIRLO	Zr–1.0Nb–1.0Sn–0.1Fe	Sheet and tube	
Zircaloy-4	Zr–1.45Sn–0.2Fe–0.1Cr	Sheet and tube	650–700

Table 2
Processing steps for the model alloys.

Processing step	Model alloys
Vacuum arc melt	Melt 4 times to promote chemical homogeneity
Beta phase heat treatment	β-Anneal
	Water quench
Hot roll	580 or 720 °C
	Roll to ~4 mm
Condition	Grit blast to remove oxide, pickle
Vacuum anneal	580 or 720 °C for 4 h
Condition	Pickle
Cold roll	Roll to ~2 mm
Vacuum anneal	580 or 720 °C for 4 h
Condition	Pickle
Cold roll	Roll to ~0.8 mm
Final vacuum anneal	580 or 720 °C for 2–4 h
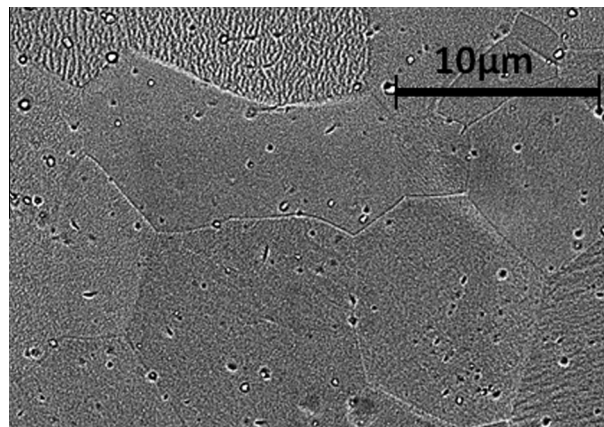
Fig. 1. Scanning electron microscope micrograph of Zircaloy-4 sheet cross section with the transverse direction being normal.

heat treatment (Fig. 1), except for Zircaloy-4 tube in a CWSR state showing elongated grains (Fig. 2). The holes in Figs. 1 and 2 are preferentially etched precipitates. ZIRLO and Zr–2.5Nb alloys show microstructure similar to that observed in Fig. 1 with a higher precipitate volume fraction. The precipitates appear to be distributed homogeneously and are generally equiaxed except for the elongated precipitates observed in Zr–2.5Nb–05Cu and Zr–0.5Cu (Fig. 3). The consistent presence of copper in these elongated precipitates has been confirmed by EDS.

From optical micrographs of Zr–0.4Fe–0.2Cr (Fig. 4), the Zr–0.4Fe–0.2Cr alloy grain size annealed at 580 °C is smaller than that of alloys heat treated at 720 °C [17]. The α-Zr average grain diameter was measured to be approximately equal to 10 μm. The average precipitate diameter measured using synchrotron X-ray diffraction is 40 nm in Zr–0.4Fe–0.2Cr (L) and 110 nm in Zr–0.4Fe–0.2Cr (H) [17].
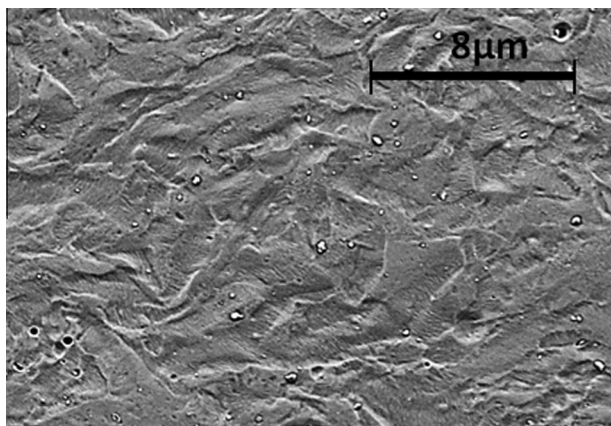
Fig. 2. Scanning electron microscope micrograph of Zircaloy-4 tube cross section with the transverse direction being normal.
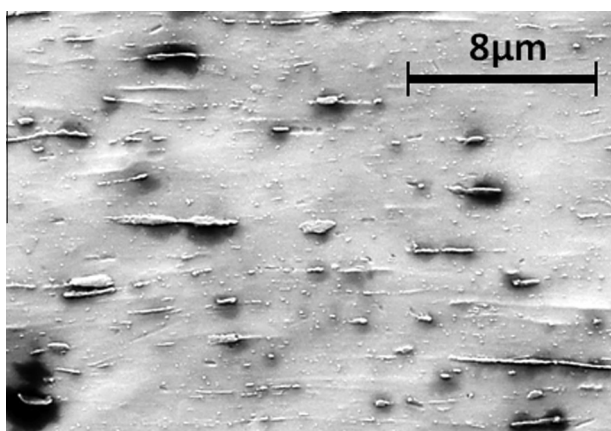
Fig. 3. Scanning electron microscope micrograph of Zr–2.5Nb–0.5Cu tube cross section with the longitudinal direction being normal.

2.2. Corrosion test

Corrosion tests were performed at Westinghouse Electric Co. Multiple corrosion coupons of each alloy were corroded in 360 °C pure water at saturation pressure of 18.7 MPa (2708.6 psi) in accordance with ASTM G2 [18]. The autoclave was periodically opened to measure the sample weight gains as a function of exposure time and to archive specimens for subsequent measurement of hydrogen by VHE. The periodic opening of the autoclave helped maintain low dissolved hydrogen levels (less than 50 cc H_2/kg H_2O) in the autoclave throughout the experiment by refreshing the autoclave solution at the start of each corrosion interval. Hydrogen levels in water less than 25–50 cc of H_2/(kg of H_2O) should have no impact on the corrosion process [2].
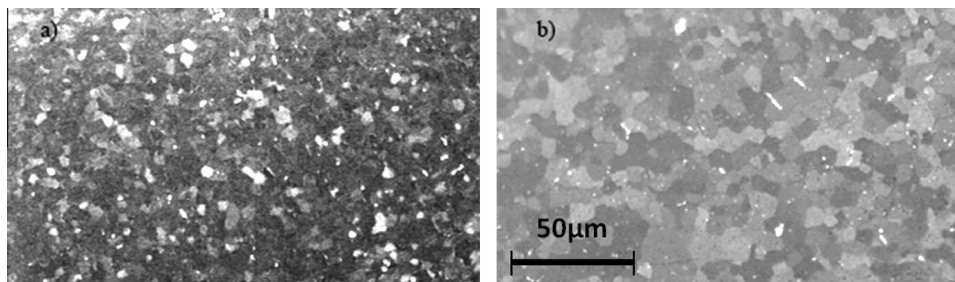
In addition to hydrogen measurements in the archived samples by VHE, some additional samples were used for hydrogen measurements by CNPGAA. Since this experiment measures hydrogen content non-destructively, these samples were returned to the autoclave for additional exposure followed by further CNPGAA measurements of hydrogen concentrations. This allowed following the evolution of hydrogen pickup fraction as a function of exposure time *on a single sample.*

2.3. Hydrogen measurements

VHE measurements were performed by LUVAK, Inc. in Boylston, MA, using an NRC Model 917 apparatus [19] as described in detail in a previous paper [15]. Although this technique is fast and reasonably accurate, it is also destructive. To measure the hydrogen content as a function of time, it is necessary to perform measurements on different (sister) samples from the same alloy, which is a potential source of measurement dispersion. Duplicate measurements from the same coupon confirmed that the average measurement error is approximately equal to ±10%, as confirmed by other studies [14,20]. The total analyzed sample size was 8 mm × 8 mm for sheet coupons and 3 mm-long tube sections for tube coupons. The analyzed samples were made as large as possible to minimize any local area-to-area variations of hydrogen content which is another potential source of measurement dispersion.

CNPGAA measurements in zirconium alloys have already been discussed in detail elsewhere [15]. CNPGAA was performed at National Institute of Standards and Technology (NIST), Gaithersburg, MD, in one of the cold neutron beam lines on various sheet samples. The background noise at the hydrogen gamma ray energy at this beamline was very low so that concentrations of hydrogen in zirconium alloys as low as 5 wt ppm are detectable. The gamma-ray spectra were fit using two different programs: an algorithm for hand fitting of peaks (SUM) written at NIST [21] and the standard commercial peak search program Genie2000®.

2.4. Hydrogen pickup fraction

The *total hydrogen pickup fraction f_H^t* is defined as the ratio of the hydrogen absorbed from the beginning of the corrosion test to the total amount of hydrogen generated by the corrosion reaction:

$$f_H^t = \frac{\Delta_0^t H_{absorbed}}{\Delta_0^t H_{generated}} \tag{3}$$

The hydrogen pickup fraction of a sample was calculated from measurement of both weight gain and hydrogen content. The assumptions made for calculations of hydrogen pickup fraction are the following:

- The oxide formed during autoclave exposure did not spall, so that the measured weight gain was a valid measurement of the extent of oxide formation. This was confirmed by visual inspection of the specimens.

Fig. 4. Polarized light microscopy micrographs of (a) Zr–0.4Fe–0.2Cr (L) annealed at 580 °C and (b) Zr–0.4Fe–0.2Cr (H) [17].

- The weight gain is assumed to be only due to oxygen and does not take into account the hydrogen uptake. This is a good assumption for low hydrogen pickup fraction but it should be kept in mind that the hydrogen uptake resulting from a theoretical hydrogen pickup fraction of 100% would account for 11.1% of the weight gain.
- Finally the hydrogen that enters the sample comes only from the hydrogen generated during the corrosion reaction. This assumption is mostly valid in autoclave corrosion, since no radiolysis of water occurs, in contrast to in-reactor conditions. Also, since the autoclave was opened at least every 30 days, no significant build-up of hydrogen gas is observed in the autoclave (the concentration was kept below 50 cc H_2/kg H_2O) so that hydrogen evolved from one sample does not enter the other samples as confirmed in [22]. At the early stages of corrosion when corrosion rates are higher and hydrogen gas releases are more significant, the autoclave was opened more frequently.

According to these assumptions, the concentration (in wt ppm) of hydrogen in the sample C_H^t is given by the following equation:

$$C_H^t = 10^6 \frac{m_H^c + m_H^i}{m_s^t} \tag{4}$$

where m_s^t is the mass of the sample at the time of the measurement, m_H^i is the initial mass of hydrogen in the sample and m_H^c is the mass of hydrogen picked up by the sample during corrosion. m_H^c is equal to:

$$m_H^c = \frac{2N_O f_H^t}{N_A} M_H \tag{5}$$

where N_A is Avogadro's number, M_H the atomic mass of hydrogen and N_O the number of oxygen atoms absorbed into the sample during corrosion. N_O is equal to:

$$N_O = \frac{(m_s^t - m_s^i)}{M_O} N_A \tag{6}$$

where m_s^i the initial sample mass and M_O the atomic mass of the oxygen atom.

The initial mass of hydrogen (in grams) in the sample is given by $m_H^i = C_H^i m_s^i \times 10^{-6}$ where C_H^i is the initial concentration of hydrogen in the sample in wt ppm. If C_H^t is the concentration of hydrogen at the time of measurement in wt ppm (see Eq. 4), f_H^t is equal to:

$$f_H^t = \frac{10^{-6}(m_s^t C_H^t - m_s^i C_H^i)}{2 \frac{(m_s^t - m_s^i)}{M_O} M_H} \tag{7}$$

The *instantaneous hydrogen pickup fraction* f_H^i is defined as the ratio of the hydrogen absorbed between time t and time $t + \Delta t$ to the total amount of hydrogen generated by the corrosion reaction during the same time increment. Mathematically it is the time derivative of the hydrogen absorbed divided by the time derivative of the amount of hydrogen generated during corrosion:

$$f_H^i = \frac{\frac{dH_{absorbed}}{dt}}{\frac{dH_{generated}}{dt}} \sim \lim_{t \to 0} \frac{\Delta_t^{t+\Delta t} H_{absorbed}}{\Delta_t^{t+\Delta t} H_{generated}} \propto \frac{dH_{absorbed}}{d\delta} \tag{8}$$

where δ is the oxide thickness. For clarity it is emphasized that f_H^i is not the time derivative of f_H^t, but it does reflect the hydrogen pickup fraction over a smaller time increment rather than the total time as in f_H^t. There have been few measurements of instantaneous hydrogen pickup fraction in the past since it requires precise hydrogen measurements at successive small time intervals [14]. Nevertheless, the measurements of f_H^i is very useful to describe hydrogen pickup kinetics. However, the use of sister samples can introduce variability in the determination of f_H^i, hence the need for the development

of a non-destructive technique to precisely and accurately determine f_H^i on a single sample.

From Eq. 7 f_H^i is also given by:

$$f_H^i = \frac{10^{-6}(m_s^{t+\Delta t} C_H^{t+\Delta t} - m_s^t C_H^t)}{2 \frac{(m_s^{t+\Delta t} - m_s^t)}{M_O} M_H} \tag{9}$$

The errors in the measurement of the hydrogen pickup fraction errors were determined using error propagation methods.

3. Results

3.1. Corrosion test

The weight gains are plotted as a function of exposure time for the different alloys in Fig. 5. These weight gains are the average weight gains from the duplicate samples at each corrosion interval. The standard deviation of the weight gain measurements was less than 0.5 mg/dm² for the production alloys (Fig. 5a–f). The production alloys show the transition type corrosion behaviour that has often been observed in zirconium alloys [23].

The weight gains of the four model alloys as function of exposure time are also plotted in Fig. 5g–j (with different exposure time scales). The two Zr–0.4Fe–0.2Cr alloys (i and j) do not show evidence of oxide transition in the exposure time studied so that their oxides are expected to be still protective after 463 days. The corrosion data of Zr–0.5Cu (respectively pure Zr) are only shown in the protective regime. After 233 days (respectively 14 days for pure Zr) the alloys underwent a sudden breakaway after which their oxide layers ceased to be protective. The loss of protectiveness of Zr–0.5Cu and pure Zr has been confirmed by SEM characterizations of the oxide layers. Lateral and longitudinal cracks as well as significant preferential oxide growth in the zirconium metal (under the form of dendrites) were observed in these oxide layers after breakaway [17]. However, before breakaway, the oxide layers do not show any cracks and are still adherent to the metal, so that the hydrogen pickup fraction calculations are valid.

It has been reported that the general oxidation kinetics follows a power law: $\delta = Kt^n$ [17,24–26]. By fitting the weight gain data to a power law, the exponent n has been determined for the various zirconium alloys in this study. An example of this fit is displayed in Fig. 6 and the values of n are displayed in Table 3 for the other alloys. The gray area on the plot represents the error associated to the power law fit to enclose all experimental data points and is equal to ±5% in this case. The oxide thicknesses (determined from weight gain measurements 1 μm = 14.77 mg/dm²) at the first transition δ_t for the production alloys were determined by extrapolation of the weight gain measurements by fitting the pre-transition and the 1st transition regime to power laws. The oxide thicknesses at transition δ_t are displayed in Table 4 for the different alloys. The extrapolation of the oxide thickness at the 2nd transition is less obvious because of the lack of samples at long exposure times but was possible for some of the alloys, as seen in Table 4.

3.2. Total hydrogen pickup fraction

The hydrogen content as function of exposure time can be fitted empirically with a polynomial of the lowest degree to allow good fitting of the data. This polynomial has no physical significance but is only used to fit the data and carry out hydrogen pickup fraction calculations. By trial and error, a 4th degree polynomial function was found to be optimal for every alloy and transition regime. Indeed, a 3rd degree or lower polynomial does not reproduce either the hydrogen content variations as function of exposure time or f_H^t measured experimentally as detailed next. On the other hand, a 5th degree or higher polynomial does not significantly
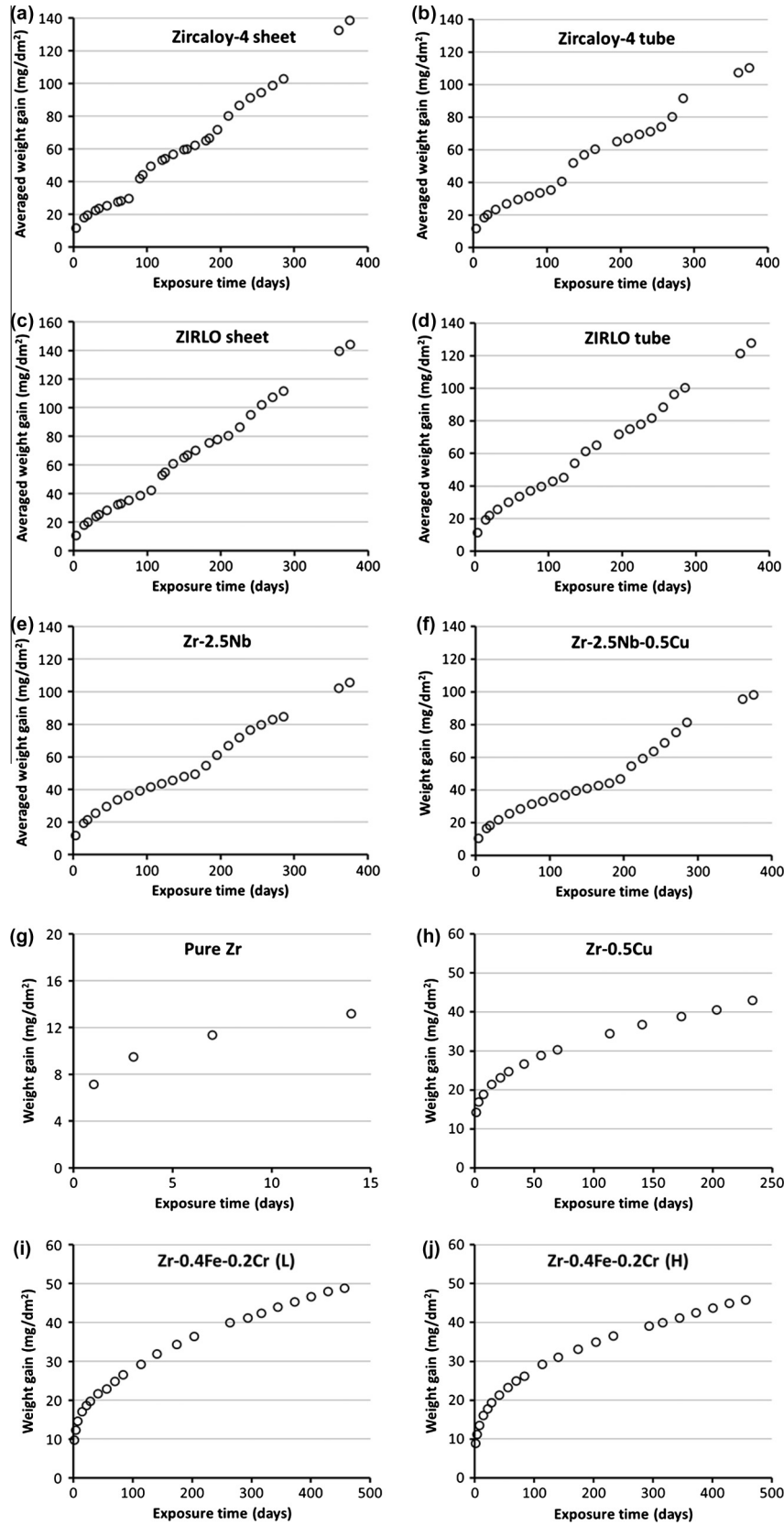
Fig. 5. Weight gain as a function of exposure time for the following production alloys: (a) Zircaloy-4 sheet, (b) Zircaloy-4 tube, (c) ZIRLO sheet, (d) ZIRLO tube, (e) Zr–2.5Nb, (f) Zr–2.5Nb–0.5Cu, and model alloys (g) pure Zr, (h) Zr–0.5Cu, (i) Zr–0.4Fe–0.2Cr (L), (j) Zr–0.4Fe–0.2Cr (H).
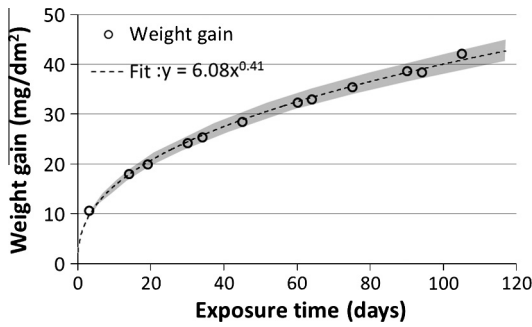
Fig. 6. Power law fit of the pre-transition regime of ZIRLO sheet alloy. The shaded area represents ±5% of the weight gain determined by the fit.

Table 3
Exponent n from pre-transition (or pre-breakaway) power law fits of the different alloys [17].

Alloy	Exponent n
Pure Zr	0.20
Zr–0.4Fe–0.2Cr (L)	0.21
Zr–0.4Fe–0.2Cr (H)	0.23
Zr–0.5Cu	0.17
Zr–2.5Nb	0.37
Zr–2.5Nb–0.5Cu	0.36
ZIRLO sheet	0.41
ZIRLO tube	0.37
Zircaloy-4 sheet	0.29
Zircaloy-4 tube	0.32

Table 4
Extrapolated oxide thickness at the 1st transition δ_t and 2nd transition for different alloys.

Alloy	Oxide thickness at the 1st transition (μm) δ_t	Oxide thickness at the 2nd transition (μm)
Zr–2.5Nb	3.5	
Zr–2.5Nb–0.5Cu	3.2	
ZIRLO sheet	2.9	5.7
ZIRLO tube	3.1	
Zircaloy-4 sheet	2.1	4.5
Zircaloy-4 tube	2.6	4.9

modify the fit and would introduce unphysical variations of the hydrogen content as function of exposure time. An example of a fit using a 4th order polynomial is displayed in Fig. 7. The gray area represents the error associated to the polynomial fit to enclose all experimental data points and is equal to ±10% in this case.

f_H^t can be determined at given exposure times using the experimental data from archived samples and also continuously using the functions from the weight gain and hydrogen content fits (Eq. 7). The hydrogen content fits were not carried out on the model alloys because of the sparseness of the data, so only the experimentally measured f_H^t are plotted for these alloys. The f_H^t results are plotted in Fig. 8 for the production alloys and Fig. 9 for model alloys.

The production alloys in Fig. 8 show a common general trend, independent of the alloy. At the very start of the corrosion process, f_H^t increases markedly before reaching a plateau. Then, approximately halfway before transition, f_H^t starts steadily increasing again up to transition and showing an apparent decrease just before the transition. This evolution repeats itself in the next transition regime, suggesting that the hydrogen pickup kinetics follow the periodicity of the oxidation kinetics periodicity but with different behaviour [17,27]. Finally, it is noted that f_H^t increases from one
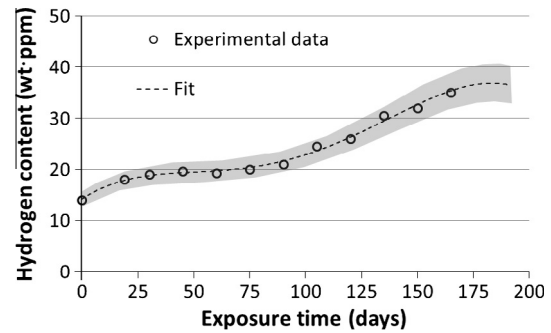
Fig. 7. Fit of the hydrogen pickup kinetics using a 4th polynomial function for the case of the Zr–2.5Nb alloy in pre-transition regime. The shaded area represents ±10% of the hydrogen content determined by the fit.

transition regime to the next, suggesting that although the protective oxide behaves similarly from one period to the next, the nonprotective oxide present after the first transition affects the hydrogen pickup process. Although it is not expected that the f_H^t will keep increasing indefinitely with successive periods it is not possible to determine the final steady state value because of the lack of archived samples at very long exposure times.

Fig. 9 shows the measurements of hydrogen pickup in the model alloys. Even though the data are more scattered, a similar f_H^t evolution is observed for the Zr–0.4Fe–0.2Cr alloys as for the production alloys. Comparing f_H^t of different alloys together using Figs. 8 or 9 is not easy since all the alloys have different oxidation kinetics.

Thus, it is useful to plot the results in a manner that allows easier comparison of f_H^t of different alloys with similar oxide thickness, but different kinetics. The hydrogen contents (in mg/dm^2) of zirconium alloys are plotted in Figs. 10a–10d as function of weight gain (the corresponding oxide thickness is also indicated at the top). An expanded view at low weight gain results is provided in Figs. 10a and 10b for clarity. Results obtained with CNPGAA are indicated by a star. In such a plot, constant f_H^t results in a straight line and thus the dashed lines represent constant values of f_H^t of 10%, 20%, 30% and 40%. Since the experimental values do not follow straight lines, the results clearly show that (i) f_H^t varies from alloy to alloy, and (ii) for a given alloy f_H^t increases with increasing exposure time.

Fig. 10a shows that the f_H^t of pure Zr at 1 μm (before breakaway) is approximately equal to 18%. This pickup fraction is higher than that of any other alloys before the transition, except for Zr–0.5Cu (see Fig. 10c). In the pre-transition regime (before 1st transition) Zircaloy-4 exhibits a much lower f_H^t (~8%) than pure Zr. Zircaloy-4 reaches similar f_H^t than pure Zr only after growing an oxide of 5.5 μm. These observations suggest that the presence of alloying elements reduces hydrogen pickup fraction [7]. In the case of Zircaloy 4 this effect is likely ascribed to precipitates since Sn has been previously shown to have limited effect on hydrogen pickup [7]. In Fig. 10c, for an oxide thickness of approximately 3 μm, the f_H^t for Zr–0.5Cu is equal to 25% compared to 15% for Zr–2.5Nb–0.5Cu and 5% for Zr–2.5Nb. Thus it appears that at a given oxide thickness the addition of Cu in zirconium alloys increases f_H^t, whereas Nb addition decreases it. The f_H^t of Zircaloy-4 and ZIRLO lies between the f_H^t of Zr–2.5Nb and the f_H^t of Zr–2.5Nb–0.5Cu, with a constantly lower f_H^t for ZIRLO compared to that of Zircaloy-4 at a given weight gain (see Figs. 10a and 10b).

It is also observed that f_H^t increases with oxide thickness. At the end of the corrosion test (after 375 days of corrosion), there is some indication that the f_H^t of Zircaloy-4 and ZIRLO start to stabilize around 25% for Zircaloy-4 and 19% for ZIRLO. At the end of the corrosion test, Zr–2.5Nb alloy shows the lowest f_H^t (~15%)
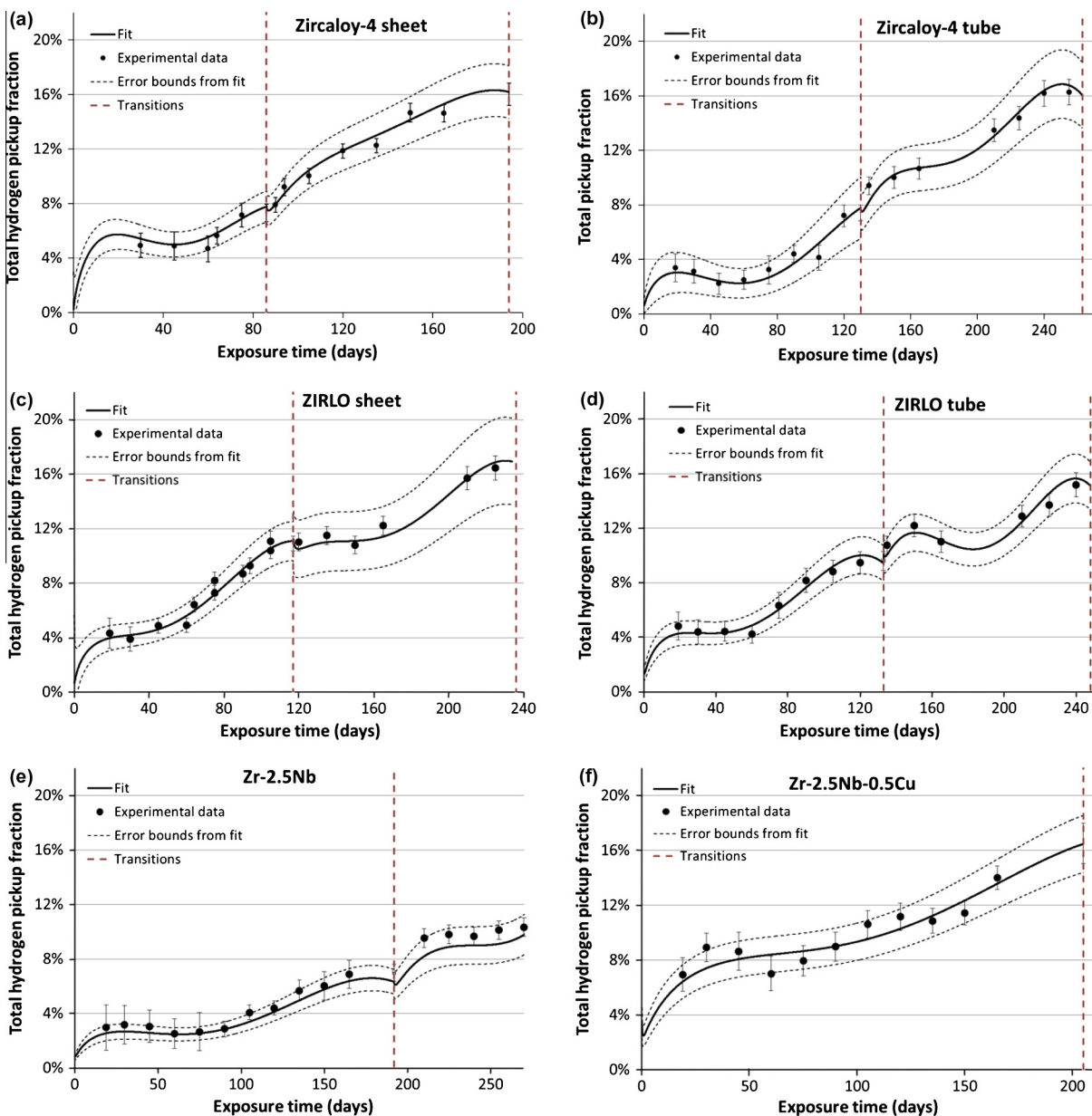
Fig. 8. Total hydrogen pickup fraction (determined experimentally and from the weight gain and hydrogen content fits) as function of exposure time of (a) Zircaloy-4 sheet, (b) Zircaloy-4 tube, (c) ZIRLO sheet, (d) ZIRLO tube, (e) Zr–2.5Nb, (f) Zr–2.5Nb–0.5Cu. The transitions and the errors from the fits are also indicated.

whereas Zr–2.5Nb–0.5Cu shows the highest f_H^t ($\sim$35%). For these alloys the f_H^t increases more from the 1st transition to the 2nd, than, from the 2nd to the 3rd.

The microstructure of the alloy also affects f_H^t. In Fig. 10d, the hydrogen content as function of weight gain is plotted for the Zr–0.4Fe–0.2Cr model alloys. Before reaching an oxide thickness of approximately 3 μm, the alloys show a similar f_H^t (between 10% and 15%). Fig. 5 shows that beyond that oxide thickness, an increase in f_H^t is observed in both alloys even though the corrosion kinetics is unchanged and the oxide layers observed by SEM are identical (no significant cracks are present). This increase is more marked in the alloy with smaller precipitates. At the end of the corrosion test, even though both alloys have approximately the same oxide thickness, the f_H^t of Zr–0.4Fe–0.2Cr (H) is equal to 20% whereas the f_H^t of Zr–0.4Fe–0.2Cr (L) is above 30%. This suggests that for Zr–0.4Fe–0.2Cr alloy type, for a given volume fraction and corrosion rate, alloys with larger precipitates tend to pick up less hydrogen than alloys with smaller precipitates.

Not only the precipitate size but also the general microstructure can affect the results. It is observed that the tube geometry delays the oxide transition compared to the sheet geometry, probably because of a better stress accommodation. However, the geometry or the metallurgical state of the alloy (recrystallized or not) do not seem to affect the hydrogen pickup fraction.

3.3. Instantaneous hydrogen pickup fraction

It is clear from Figs. 8–10 that f_H^t varies within a given period. Accordingly, f_H^i was calculated in order to more precisely characterize this evolution as function of oxidation kinetics. f_H^i can be approximated from experimental data either by VHE on sister samples or by CNPGAA on a given sample. These calculations have only been performed on the production alloys since the model alloys have not been consistently archived at regular time intervals. Regarding VHE measurements, the time increments between two hydrogen content measurement on sister samples have not been
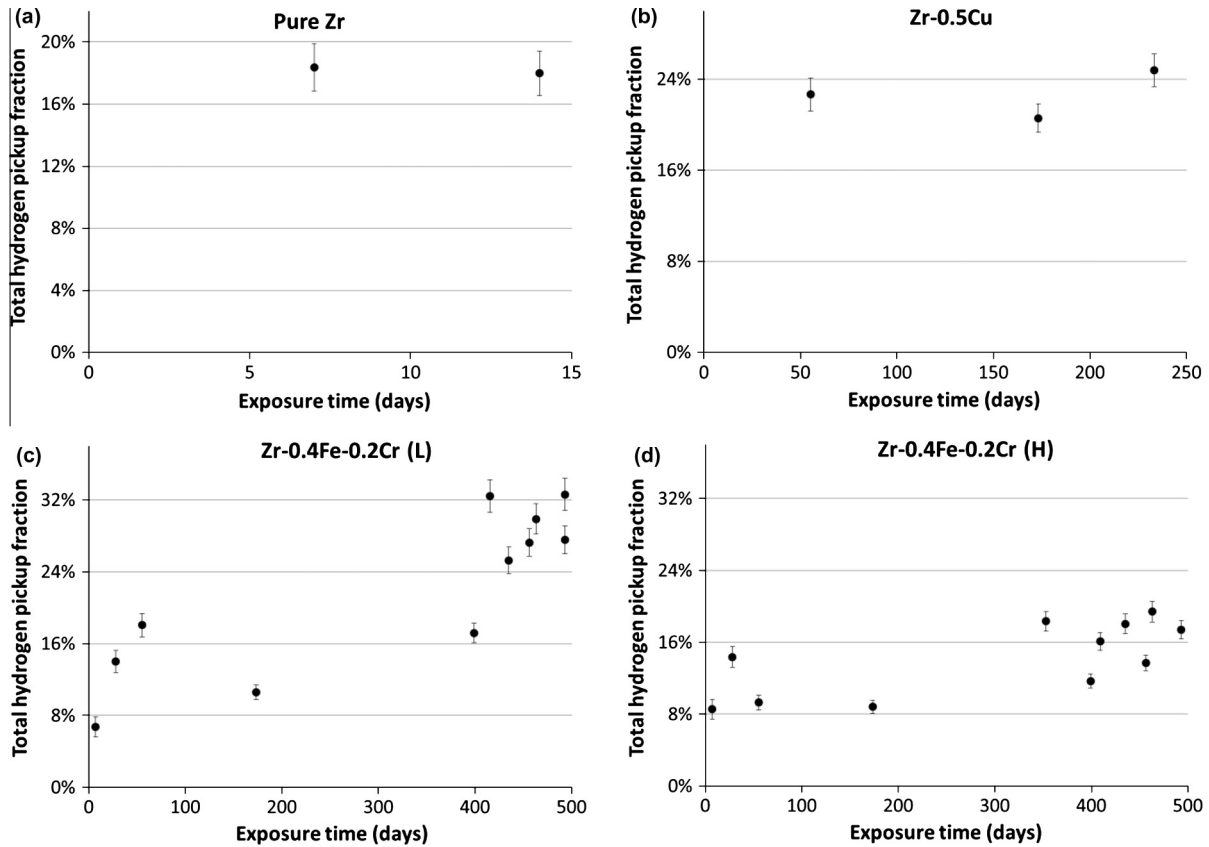
Fig. 9. Total hydrogen pickup fraction (determined experimentally) as function of exposure time of (a) pure Zr, (b) Zr–0.5Cu, (c) Zr–0.4Fe–0.2Cr (L), (d) Zr–0.4Fe–0.2Cr (H).
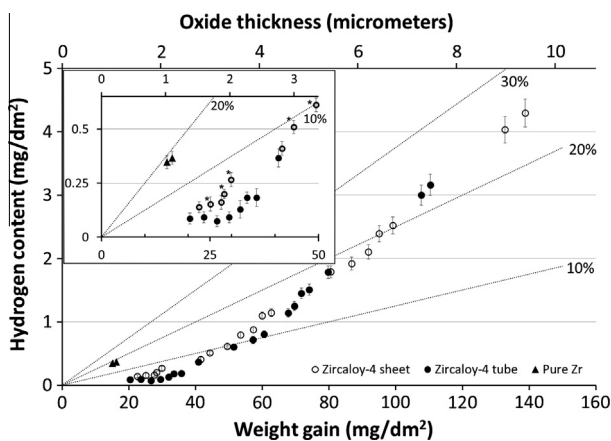
Fig. 10a. Hydrogen content (in mg/dm²) as a function of weight gain (and oxide thickness) for the Zircaloy-4 sheet and tube. The straight dashed lines correspond to constant total hydrogen pickup fraction of 10%, 20% and 30%. An expanded view at early exposure time is displayed. Results obtained with CNPGAA are marked by a star on the upper left of the symbol.
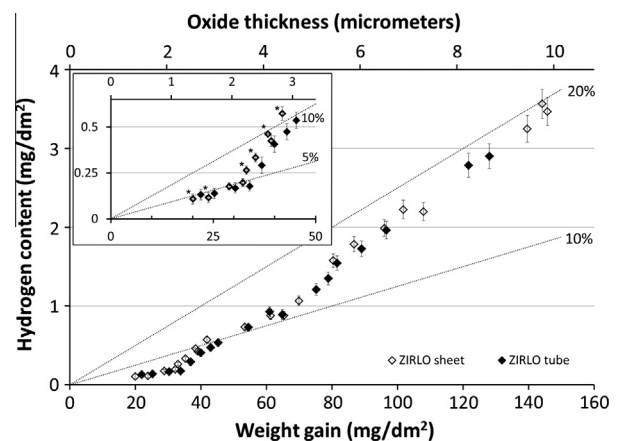
Fig. 10b. Hydrogen content (in mg/dm²) as a function of weight gain (and oxide thickness) for the ZIRLO sheet and tube. The straight dashed lines correspond to constant total hydrogen pickup fraction of 5%, 10% and 20%. An expanded view at early exposure time is displayed. Results obtained with CNPGAA are marked by a star on the upper left of the symbol.

kept constant throughout the experiment. Two sets of sister samples were used and their time intervals are listed in Table 5.

Because the variations of f_H^i as function of exposure time are similar for all the production alloys only the results on ZIRLO sheet are displayed in this paper. These time dependent or instantaneous results are plotted in Fig. 11 along with the weight gain. The large error bars in f_H^i come from the small Δt and from errors from the VHE measurements, especially when the corrosion rate is low (small changes in hydrogen content). It is clear from the data that f_H^i varies with exposure time. At first, when the corrosion rate is

high, f_H^i is low. Then, the corrosion rate slows down and f_H^i increases significantly. This steep increase in f_H^i is observed for every alloy. f_H^i keeps on increasing until the sample reaches transition. Just before transition, the f_H^i calculated from the fits appear to drop significantly for all the alloys. It is not clear if this is due to real physical phenomena or is due to the errors associated to the fitting functions used. After the 1st transition, the corrosion rate increases again and f_H^i returns to the low values observed at the beginning. Because the derivatives of the weight gain and hydrogen content fits are not continuous at transition, the derived instantaneous
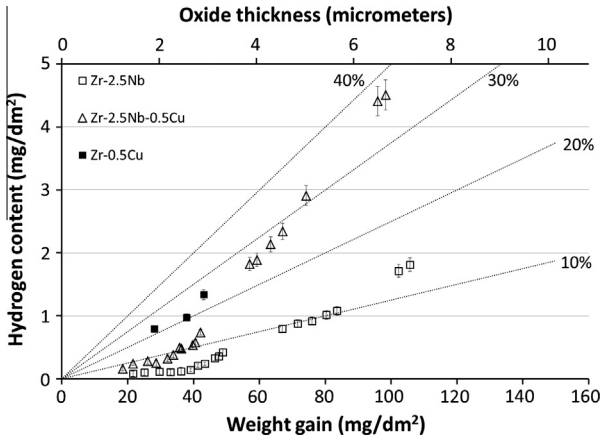
Fig. 10c. Hydrogen content (in mg/dm^2) as a function of weight gain (and oxide thickness) for the Zr–0.5Cu, Zr–2.5Nb–0.5Cu and Zr–2.5Nb. The straight dashed lines correspond to constant total hydrogen pickup fraction of 10%, 20%, 30% and 40%.
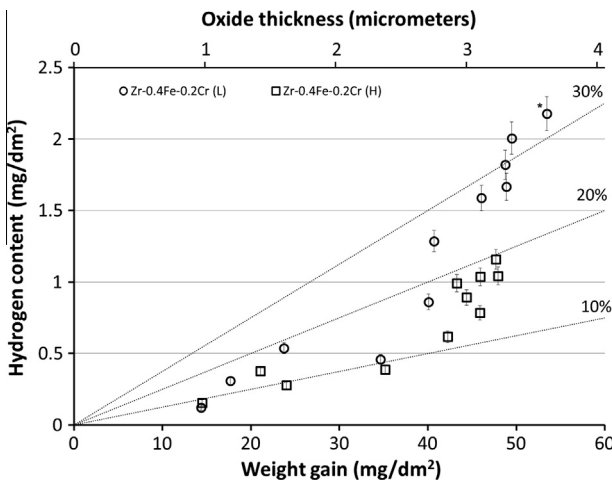
Fig. 10d. Hydrogen content (in mg/dm^2) as a function of weight gain (and oxide thickness) for the Zr–0.4Fe–0.2Cr (L) and Zr–0.4Fe–0.2Cr (H) alloys. The straight dashed lines correspond to constant total hydrogen pickup fraction of 10%, 20% and 30%. Results obtained with CNPGAA are marked by a star on the upper left of the symbol.

Table 5
Time increments between two VHE measurements and archiving of sister samples.

1st Set of sister samples	2nd Set of sister samples
0 → 19 Days	0 → 30 Days
19 → 45 Days	30 → 60 Days
45 → 75 Days	60 → 90 Days
75 → 105 Days	90 → 120 Days
105 → 135 Days	120 → 150 Days
135 → 165 Days	150 → 210 Days
165 → 225 Days	210 → 240 Days
225 → 255 Days	240 → 270 Days
225 → 375 Days	270 → 360 Days

hydrogen pickup fraction is also not continuous at transition. Then the process repeats itself in the 2nd transition regime and so on, following the periodicity of the oxidation kinetics.

In order to evaluate the possible effect of different hydrogen pickup behaviour among sister samples, CNPGAA was used to follow hydrogen pickup in two selected ZIRLO sheet samples at different exposure times. These single samples had their hydrogen content measured at different exposure times by CNPGAA. The results are plotted in Fig. 12 and the f_H^i determined by the fits is also plotted for comparison (see Fig. 11). It is concluded that f_H^i on a single sample follows the same pattern as the one described from sister samples in Fig. 11, confirming that the general experimental conclusions on hydrogen pickup fraction evolution drawn from Fig. 11 are valid and can be rationalized to a hydrogen pickup mechanism.

To conclude, it is interesting to calculate the hydrogen uptake of a given sample in wt ppm per day. Indeed, since f_H^i increases as the oxidation rate (proportional to $\Delta^t H_{generated}$) slows down, it could be argued that the overall hydrogen uptake per day ($\Delta^t H_{absorbed}$) might be a constant (see Eq. 3). The hydrogen uptake in wt ppm per day determined by CNPGAA is plotted for ZIRLO sheet samples in Fig. 13. It is directly concluded that the hydrogen uptake rate is not a constant of exposure time. The variations being measured on a given sample, they do not result from data scattering in sister samples and thus give direct and meaningful indications on the hydrogen pickup mechanism of zirconium alloys.

The implication of these results is discussed in the following section.

4. Discussion

The total and instantaneous hydrogen pickup fraction general trends common to every alloy are plotted in Fig. 14 as function of oxide thickness relative to transition oxide thickness δ_t:

- At small oxide thickness (<40% of δ_t), f_H^i increases.
- Between 40% and 70% of δ_t, f_H^i reaches a plateau.
- Approximately at 70% of δ_t, f_H^i starts to steadily increase again up to transition.
- The decrease in f_H^i before transition might be physical or might come from the errors associated to the fitting functions used.

The results on hydrogen pickup in the previous section show that the hydrogen pickup mechanism is directly linked to the corrosion mechanism even though hydrogen pickup kinetics does not follow oxidation kinetics.

It is thus interesting to determine if there is a correlation between f_H^t and oxidation kinetics for different alloys that would suggest a common oxidation and hydrogen pickup mechanism. To compare the different alloys, since f_H^t varies inside of a transition regime and that δ_t also varies between alloys, the value of f_H^t in the plateau region (between 40% and 70% of δ_t, see Fig. 14) was used. This value is plotted as function of the parameter n (in Table 3) in Fig. 15.

An inverse relationship between the oxidation kinetics and f_H^t is observed: the lower the n, the higher the f_H^t. It is observed that the Zr–Fe–Cr and Zircaloy type alloys exhibit quadratic to cubic behaviour and higher f_H^t compared to the Nb alloys, at the end of the spectrum, which exhibit close to parabolic kinetics ($n \sim 0.4$) and the lowest f_H^t. These results definitely show that the oxidation kinetics variations between alloys are linked to the variations of f_H^t, which indicates that the hydrogen pickup mechanism is linked to the corrosion kinetics: the more the oxidation kinetics tend towards parabolic the lower the hydrogen pickup fraction. This is also in accordance with results reported on binary Zr–Fe alloys [28] and on Zr–Sn–Fe–Cr alloys [29] and with the overall lower hydrogen pickup fraction of Nb containing alloys [30]. These general results are summarized as a scheme in Fig. 16.

The f_H^t exhibits a dependency on alloying element content and on alloy microstructure. Nb addition decreases hydrogen pickup fraction whereas Cu addition increases it as observed in Fig. 10c. The beneficial effect of Nb addition on f_H^t in binary Zr–Nb alloys
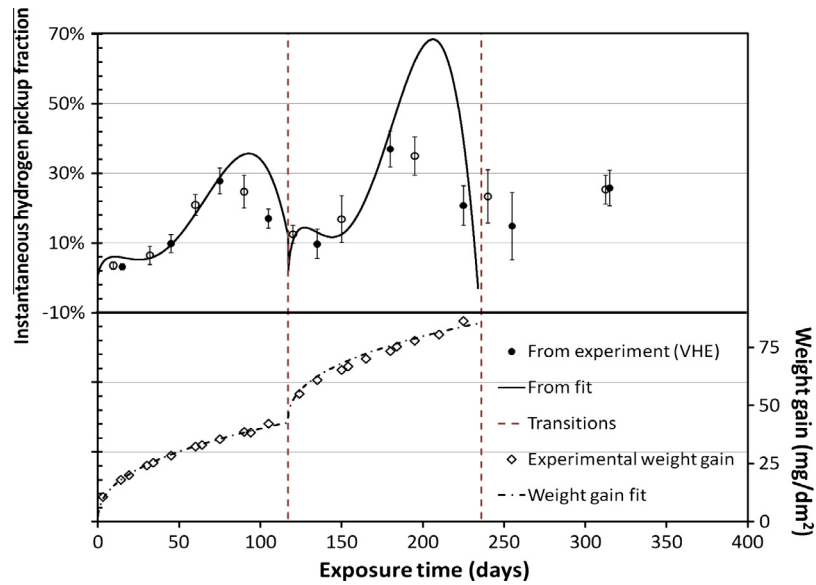
Fig. 11. Instantaneous hydrogen pickup fraction and weight gain as a function of exposure time determined experimentally for ZIRLO sheet. The weight gain fit and the instantaneous hydrogen pickup fraction determined from the weight gain and hydrogen content fits are also plotted. The data points corresponding to experimental f_H^i are positioned at the middle of the time increment.
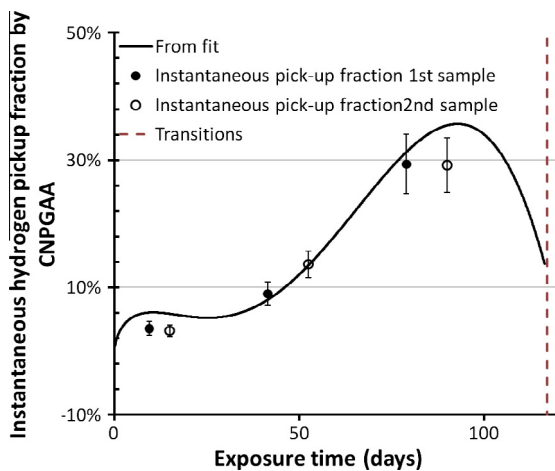
Fig. 12. Instantaneous hydrogen pickup fraction determined from CNPGAA measurements for two ZIRLO samples. The transition and the instantaneous hydrogen pickup fraction determined from the weight gain and hydrogen content fits are also plotted (see Fig. 11). The data points corresponding to experimental f_H^i are positioned at the middle of the time increment.
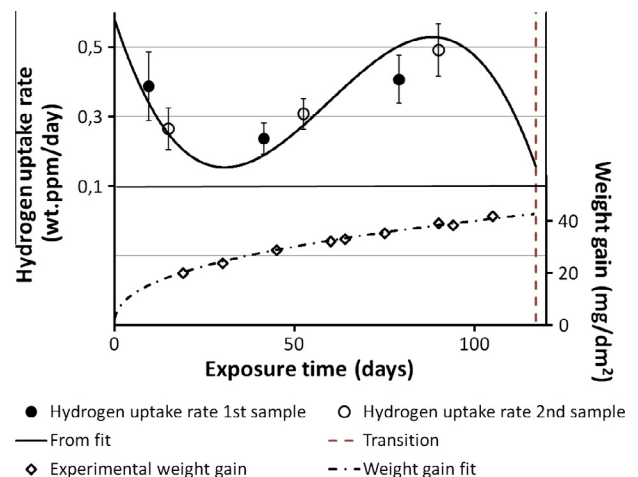
Fig. 13. Hydrogen uptake rate in wt ppm/day as function of exposure time determined from CNPGAA measurements for two ZIRLO samples. The transition and the instantaneous hydrogen uptake rate determined the hydrogen content fit are also plotted. The experimental data points are positioned at the middle of the time increment.

has already been observed [30–32]. It was shown that f_H^t decreases with Nb addition, especially in the solid solution range (up to 0.5–0.6 wt% [33]). In our study, Zr–2.5Nb has the lowest f_H^t of all the alloys investigated in this study at a given exposure time. The reason for this lower f_H^t would be that the Nb atoms dissolved in the ZrO_2 solid solution would dope the oxide layer and act as donors [34–36] with an energy level close to the conduction band. If the aggregation of alloying elements and formation of complex defects are not considered, the compensating defect of the Nb positive charge would be either zirconium vacancies or electrons. The conduction band of ZrO_2 being formed of zirconium 3d empty states and the zirconium vacancy being highly charged, it is believed that electrons are preferred as a compensating defect. This hypothesis has also been confirmed by photoelectrical analysis of passive zirconium niobium oxide layers [37]. The increase in electron concentration would result in an increase of oxide electronic

conductivity. Electrochemical study on zirconium alloys have also shown that Zr–2.5Nb has the highest electronic conductivity and the lowest hydrogen pickup when compared to Zircaloy-4 [38]. According to this picture the hydrogen pickup fraction of Zr–Nb alloys should decrease significantly with addition of Nb up to the solubility limit. The effect of additional Nb additions is unclear. Indeed, as observed in Fig. 10, ZIRLO which contains 1% of Nb has a higher f_H^t than Zr–2.5Nb. Thus, either the Nb containing precipitates are beneficial or either Fe precipitates or Sn in solid solution are detrimental in terms of hydrogen pickup.

In any case it would appear that an increase in electron concentration in the oxide layer would reduce f_H^t. Other mechanisms have been proposed to explain the beneficial effect of Nb on hydrogen pickup. Bossis et al. pointed out that the Nb would be oxidized as Nb_2O_5 at the oxide/water interface so that it would act as a local donor and reduce the hydrogen before the protons get absorbed in
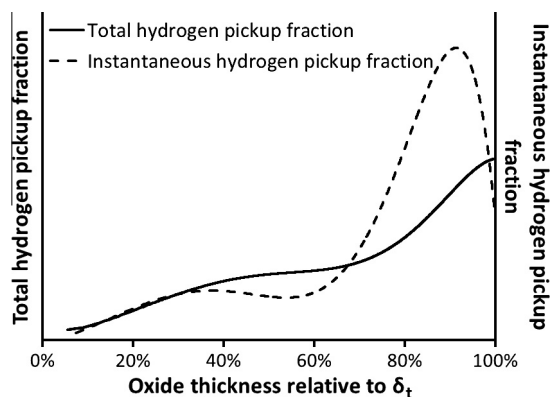
Fig. 14. Scheme of total and instantaneous hydrogen pickup fraction as function of oxide thickness relative to the oxide thickness at transition δ_t.
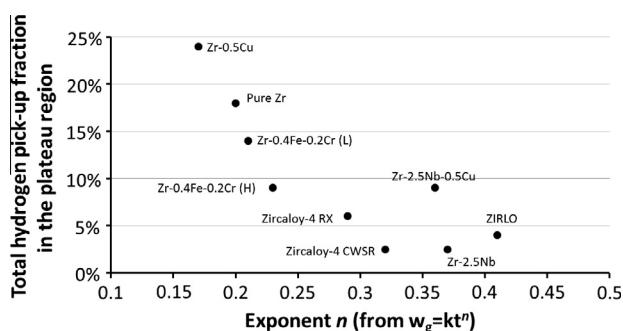
Fig. 15. Total hydrogen pickup fraction in the plateau region as function of the exponent n from the power law fit of the weight gain $w_g = kt^n$ for various zirconium alloys.
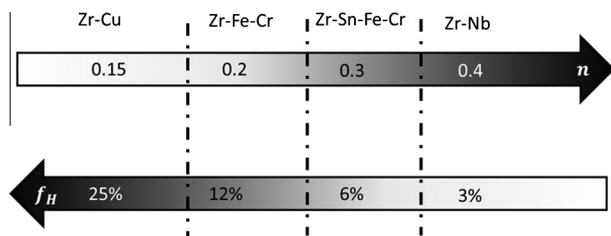
Fig. 16. Scheme of the influence of the alloying elements on oxidation kinetics (value of n) and hydrogen pickup fraction.

the oxide layer [32]. Ramasubramanian et al. calculated that the energy level of Nb_2O_5 in the ZrO_2 band gap would overlap the energy level for proton reduction at the oxide/water interface (whereas ZrO_2 conduction band is too high) and thus enhance proton reduction, reducing hydrogen pickup [39]. All these mechanisms are surface effects mechanisms and are in accordance to point out the effect of Nb on oxide electronic conductivity. However, a single surface effect cannot explain the observed variations of f_H^i in Fig. 11.

To account for the observed variations of f_H^i, an oxide property, possibly the oxide electronic conductivity, has to vary as the oxide grows. It is interesting to point out that in situ Electrochemical Impedance Spectroscopy studies have shown that the oxide resistivity followed a similar general evolution as f_H^i in this study, even the sudden drop right before transition [40,41], further indicating a possible correlation between oxide electronic conductivity and hydrogen pickup.

The Cu solid solubility limit in ZrO_2 being rather low, its acceptor effect on oxide electronic conductivity should be rather limited. The reasons why f_H^t is higher in these Cu containing alloys are still unclear, and would likely have to be sought in microstructure (especially the effect of ZrCu precipitate morphology shown in Fig. 3) and microchemistry differences rather than on the overall chemical composition.

According to the results of Fig. 10, f_H^t is also dependent on the microstructure of zirconium alloys. The presence of $Zr(Fe,Cr)_2$ precipitates appears to reduce f_H^t, compared to pure Zr. It is believed that a material with a homogeneous distribution of precipitates has a higher oxide electronic conductivity compared to pure Zr. Indeed, TEM observations [23,42] and µXANES experiments [43] have shown that Fe remains metallic (both in solid solution, with possible segregation at grain boundaries [44], and in precipitates) when incorporated into the zirconium oxide layer. Theoretical studies have also supported that $Zr(Fe,Cr)_2$ precipitates remain metallic in the oxide layer up to a certain oxide depth [45]. Metallic precipitates would likely enhance the electronic conductivity of the oxide layer, which would in turn reduce the hydrogen pickup. This argument assumes that the ZrO_2 which forms between the precipitates is also a relatively good electron conductor due to doping effects from the nearby particles since precipitates are not actually in contact.

For a given volume fraction and corrosion rate, the alloy with larger $Zr(Fe,Cr)_2$ precipitates has a lower f_H^t compared to the alloy with smaller $Zr(Fe,Cr)_2$ precipitates. Hatano et al. observed an opposite effect of precipitate size on hydrogen pickup but their study does not provide enough oxidation kinetics data and microstructure information to be totally conclusive [10]. On the other hand, electrochemical measurements [38] have shown that Zircaloy-4 with bigger precipitates (~400 nm diameter) has a lower oxide electronic resistivity than Zircaloy-4 with smaller precipitates (~130 nm diameter), which according to the authors resulted in smaller f_H^t. Even though the precipitate sizes are different in our study, this result tends to confirm our observations. However, since the heat treatment temperature of Zr–0.4Fe–0.2Cr model alloys with large and small precipitates was different, other factors besides SPP size such as the concentrations of alloying elements in the matrix, are likely different. The concentrations of alloying elements in solid solution were not quantified in this study but could also impact f_H^t.

The results in Figs. 8 and 10 indicate that the non-protective oxide may affect f_H^t since it increases from one transition regime to the next. This increase in f_H^t, already observed in [46,47], from one transition regime to the next cannot be explained by a change in the protective oxide properties since the growth of the protective oxide layer is a periodic mechanism. A likely explanation for the increase in f_H^t is that one of the boundary conditions is changing after transition. The non-protective oxide (oxide that has already gone through transition and remains on the top of the newly formed protective oxide) could affect the hydrogen pickup mechanism. It is known that hydrogen overpressure increases hydrogen pickup in zirconium alloys [11,48]. It is possible that, when the cathodic reaction occurs and hydrogen gas is released, the presence of the non-protective oxide layer between the cathodic site and the bulk water acts to create a concentration gradient of hydrogen gas across the non-protective oxide layer. The hydrogen pressure at the cathodic site would be higher compared to its value at the outer oxide water interface. In the pre-transition regime there is no hydrogen overpressure, since the cathodic site would be directly in contact with water. However, when non-protective oxide layers are present on the top of the newly formed oxide, hydrogen overpressure at the cathodic site would build-up, leading to an increase of the concentration of protons at the cathodic site. Higher concentration

of protons at the interface would therefore lead to an increase in f_H^t. This assumption should be validated by proper experimental observations of an actual increase of the hydrogen pressure at the cathodic site of post-transition oxide layers.

Finally, in light of these observations and discussions, a hydrogen pick-up mechanism based on the oxide electronic conductivity variations between alloys and as function of exposure time is under study. The corrosion mechanism should account for both oxidation kinetics and for variations in f_H^t. In order to evaluate the validity of this mechanism, the authors are currently performing X-ray Absorption Near-Edge Spectroscopy to examine the oxidation state of alloying elements in the oxide and their possible oxide doping effect and in situ Electrochemical Impedance Spectroscopy to measure the oxide electronic conductivity as function of oxide thickness. The authors are also currently studying an oxidation model based on the diffusion of charged species to evaluate the effect of oxide electronic conductivity on oxidation kinetics and hydrogen pickup driving force.

5. Conclusion

The total and instantaneous hydrogen pickup fractions from several zirconium alloys were studied. A destructive technique (VHE) was used to measure hydrogen content of samples at different exposure times. The instantaneous hydrogen pickup fraction being more sensitive to errors in the hydrogen concentration measurements, a non-destructive (and thus more precise) technique (CNPGAA) was used to measure hydrogen content. Continuous total and instantaneous hydrogen pickup fraction were calculated from careful analysis of fits of weight gains and hydrogen content measurements. Hydrogen pickup fraction variations are not caused by the build-up of hydrogen in the autoclave. The combination of both experimental techniques and the derived fits shows the following results:

- Hydrogen pickup fraction is not constant and varies as function of exposure time and between alloys.
- Hydrogen pickup fraction as function of exposure time follows a general trend common to every alloys studied in this paper:
  – At small protective oxide thickness (<40% of δ_t), f_H^i increases with exposure time.
  – Between 40% and 70% of δ_t, f_H^i reaches a plateau.
  – Above 70% of the transition thickness δ_t, f_H^i starts to steadily increase again, reaching a peak and decrease right before oxide transition.
- The hydrogen pickup fraction varies as function of oxide thickness and is non-monotonic in a transition regime.
- An inverse relationship is observed between the oxidation kinetics and f_H^t: the lower the n, the higher the f_H^t and vice versa. Zr–Fe–Cr and Zircaloy type alloys exhibit cubic kinetics and higher f_H^t compared to Nb alloys, which exhibit close to parabolic kinetics ($n \sim 0.4$) and lower f_H^t.

From these observations, we can conclude that the hydrogen pickup mechanism is directly linked to the corrosion mechanism even though hydrogen pickup kinetics does not follow oxidation kinetics.

Alloying additions have a profound impact on the hydrogen pickup mechanism:

- Nb reduces hydrogen pickup fraction whereas Cu increases it. It is proposed that the donor effect of Nb in solid solution is responsible for reducing hydrogen pickup fraction. The reasons why Cu addition increases hydrogen pickup fraction compared to other alloys with a similar oxide thickness are yet to be determined.

- Also alloy with coarser $Zr(Fe,Cr)_2$ precipitates exhibits a lower hydrogen pickup fraction than an alloy with smaller $Zr(Fe,Cr)_2$ precipitates.

Finally, hydrogen pickup fraction variations follow the periodicity of oxidation kinetics. However, the hydrogen pickup fraction increases from one transition regime to the next, indicating a possible influence of the non-protective oxide on the hydrogen pickup mechanism. The effect of hydrogen overpressure at the cathodic site has been identified as a possible cause of this hydrogen pickup fraction increase.

The authors are currently performing dedicated experiments and modeling to evaluate the different hypotheses proposed in this paper to rationalize the hydrogen pickup fraction characteristics observed.

Acknowledgements

References

[1] A.T. Motta, L.Q. Chen, JOM 64 (2012) 1403–1408.
[2] Corrosion of Zirconium Alloys in Nuclear Power Plants, IAEA-TECDOC-684, Vienna, 1993.
[3] Waterside Corrosion of Zirconium Alloys in Nuclear Power Plants, IAEA-TECDOC-996, Vienna, 1998.
[4] B. Cox, J. Nucl. Mater. 336 (2005) 331–368.
[5] S. Kass, J. Electrochem. Soc. 107 (1960) 594–597.
[6] H.H. Klepfer, Corrosion 19 (1963) 285.
[7] W.E. Berry, D.A. Vaughan, E.L. White, Corrosion 17 (1961) 109.
[8] B. Cox, J. Nucl. Mater. 264 (1999) 283–294.
[9] S. Kass, W.W. Kirk, ASM Trans. Q. 55 (1962) 77–100.
[10] Y. Hatano, M. Sugisaki, K. Kitano, M. Hayashi, Role of intermetallic precipitates in hydrogen transport through oxide films on zircaloy, in: Zirconium in the Nuclear Industry: Twelfth International Symposium, ASTM STP 1354, Philadelphia, 2000, pp. 901–917.
[11] E. Hillner, AEC Res. Develop. (1964). WAPD-TM-411.
[12] R. Adamson, F. Garzarolli, B. Cox, A. Strasser, P. Rudling, Corrosion Mechanisms in Zirconium Alloys, A.N.T. International, 2007.
[13] B. Cox, Zirconium Intermetallics and Hydrogen Uptake During Corrosion, Chalk River Nuclear Laboratories, Reactor Materials Division, 1987 (AECL Report 9383).
[14] M. Harada, R. Wakamatsu, The effect of hydrogen on the transition behavior of the corrosion rate of zirconium alloys, in: Zirconium in the Nuclear Industry: 15th International Symposium, ASTM STP 1505, 2008, p. 384.
[15] A. Couet, A.T. Motta, R.J. Comstock, R.L. Paul, J. Nucl. Mater. 425 (2012) 211–217.
[16] G.P. Sabol, R.J. Comstock, R.A. Weiner, P. Larouere, R.N. Stanutz, In-reactor corrosion performance of ZIRLO and Zircaloy-4, in: Zirconium in the Nuclear Industry: 10th International Symposium, ASTM STP 1245, Baltimore, 1994, pp. 724–744.
[17] A.T. Motta, M.J. Gomes Da Silva, A. Yilmazbayhan, R.J. Comstock, Z. Cai, B. Lai, Microstructural characterization of oxides formed on model Zr alloys using synchrotron radiation, in: Zirconium in the Nuclear Industry: 15th International Symposium, ASTM STP 1505, 2009, p. 486.
[18] Standard Test Method for Corrosion Testing of Products of Zirconium, Hafnium, and Their Alloys in Water at 680°F or in Steam at 750°F, ASTM G2/G2M-06, ASTM International, West Conshohocken, PA, 2011.
[19] Methods of Chemical Analysis of Zirconium and Zirconium Alloys (Silicon, Hydrogen, and Copper), ASTM E146-83.
[20] H. Wiese, Fractionated Determination of Hydrogen in Corroded Zirconium Alloys, PhD Thesis, Paul Scherrer Institute, Villigen, 1999.
[21] R. Lindstrom, Biol. Trace Elem. Res. 43–45 (1994) 597–603.
[22] B. Cox, C. Roy, The Use of Tritium as a Tracer in Studies of Hydrogen Uptake by Zirconium Alloys, Atomic Energy of Canada Ltd., Chalk River Nuclear Laboratories, 1965 (Report 2519).
[23] A. Yilmazbayhan, A.T. Motta, R.J. Comstock, G.P. Sabol, B. Lai, Z. Cai, J. Nucl. Mater. 324 (2004) 6–22.

[24] H.A. Porte, J.G. Schnizlein, R.C. Vogel, D.F. Fischer, J. Electrochem. Soc. 107 (1960) 506–515.

[25] K. Hauffe, Oxidation of Metals, Plenum Press, 1965.

[26] A.T. Fromhold, Theory of Metal Oxidation, North Holland Pub. Co., 1975.

[27] J.S. Bryner, J. Nucl. Mater. 82 (1979) 84–101.

[28] T. Murai, K. Isobe, Y. Takizawa, Y. Mae, Fundamental study on the corrosion mechanism of Zr–0.2Fe, Zr–0.2Cr and Zr–0.1Fe–0.2Cr alloys, in: Zirconium in the Nuclear Industry: 12th International Symposium, ASTM STP 1354, 2000, pp. 623–640.

[29] Y. Broy, F. Garzarolli, A. Seibold, L.F. Van Swam, Influence of transition elements Fe, Cr, and V on long-time corrosion in PWRs, in: Zirconium in the Nuclear Industry: 12th International Symposium, ASTM STP 1354, 2000, pp. 609–622.

[30] A.A. Kiselev, Research on the Corrosion of Zirconium Alloys in Water and Steam at High Temperature and Pressure, Atomic Energy of Canada Limited, 1963.

[31] K.-N. Choo, S.-I. Pyun, Y.-S. Kim, J. Nucl. Mater. 226 (1995) 9–14.

[32] P. Bossis, D. Pecheur, K. Hanifi, J. Thomazet, M. Blat, Comparison of the high burn-up corrosion on M5 and low tin Zircaloy-4, in: Zirconium in the Nuclear Industry: Fourteenth International Symposium, ASTM STP 1467, 2005, pp. 494–524.

[33] J.P. Abriata, J.C. Bolcich, Bull. Alloy Phase Diagrams 3 (1982) 1710–1712.

[34] A. Couet, A.T. Motta, B. De Gabory, Z. Cai, J. Nucl. Mater., in press.

[35] P. Kofstad, Nonstoichiometry, Diffusion, and Electrical Conductivity in Binary Metal Oxides, Wiley-Interscience, New York-London-Sydney-Toronto, 1972.

[36] K. Sakamoto, K. Une, M. Aomi, K. Hashizume, Oxidation behavior of niobium in oxide layers of zirconium–niobium alloys, in: Top Fuel 2012, Manchester, UK, 2012, 297-306.

[37] B.-Y. Kim, C.-J. Park, H.-S. Kwon, J. Electroanal. Chem. 576 (2005) 269–276.

[38] K. Baur, F. Garzarolli, H. Ruhmann, H.-J. Sell, Electrochemical examinations in 350 °C water with respect to the mechanism of corrosion-hydrogen pickup, in: Zirconium in the Nuclear Industry: Twelfth International Symposium, ASTM STP 1354, 2000, pp. 836–852.

[39] N. Ramasubramanian, P. Billot, S. Yagnik, Hydrogen evolution and pickup during the corrosion of zirconium alloys: a critical evaluation of the solid state and porous oxide electrochemistry, in: Zirconium in the Nuclear Industry: Thirteenth International Symposium, ASTM STP 1423, Philadelphia, USA, 2002, pp. 222–244.

[40] J. Schefold, D. Lincot, A. Ambard, O. Kerrec, J. Electrochem. Soc. 150 (2003) B451–B461.

[41] M. Tupin, C. Bataillon, J.-P. Gozlan, P. Bossis, High temperature corrosion of Zircaloy-4, in: R.W. Bosch, D. Féron, J.P. Celis (Eds.), Electrochemistry in Light Water Reactors: Reference Electrodes, Measurement, Corrosion and Tribocorrosion Issues, European Federation of Corrosion, 2007, pp. 134–163.

[42] D. Pêcheur, F. Lefebvre, A.T. Motta, C. Lemaignan, J.F. Wadier, J. Nucl. Mater. 189 (1992) 318–332.

[43] A. Couet, A.T. Motta, R.J. Comstock, Effect of alloying elements on hydrogen pick-up in zirconium alloys, in: 17th International Symposium on Zirconium in the Nuclear Industry, ASTM STP 1543, Hyderabad, India, 2013.

[44] D. Hudson, G.D.W. Smith, Scripta Mater. 61 (2009) 411–414.

[45] C. Proff, S. Abolhassani, C. Lemaignan, J. Nucl. Mater. 432 (2013) 222–238.

[46] M. Tupin, M. Pijolat, F. Valdivieso, M. Soustelle, A. Frichet, P. Barberis, J. Nucl. Mater. 317 (2003) 130–144.

[47] H.-J. Beie, A. Mitwalsky, F. Garzarolli, H. Ruhmann, H.J. Sell, Examinations of the corrosion mechanism of zirconium alloys, in: Zirconium in the Nuclear Industry: Tenth International Symposium, ASTM STP 1245, Philadelphia, PA, 1994, pp. 615–643.

[48] B. Cox, Assessment of in-reactor corrosion models and data for Zircaloys in water, in: 2nd Int. Symp. on Environmental Degradation of Materials in Nuclear Power Systems–Water Reactors, Monterey, CA, USA, 1985, pp. 219–226.

[49] G.P. Sabol, G.R. Kilp, M.G. Balfour, E. Roberts, Development of a cladding alloy for high burnup, in: Zirconium in the Nuclear Industry: 8th International Symposium, ASTM STP 1023, San Diego, 1989, pp. 227–244.